DESIGN OF A NOISE REDUCED LARGE AXIAL FAN FOR WIND TUNNEL APPLICATION WITH CFD-BASED OPTIMIZATION – A CASE STUDY

Konrad BAMBERGER[1], Thomas CAROLUS[2]
Tilo KOZUSCHEK[3], Henrik TRYGGESON[4]

[1]*University of Siegen, Institute for Fluid- and Thermodynamic*
Paul-Bonatz-Strasse 9-11, D-57068 Siegen, Germany

[2]*Steinbeis-Transferzentrum Strömungstechnik und Strömungsmaschinen*
Im Nassen 17, 57250 Netphen, Germany

[3]*Howden Axial Fans GmbH*
Habsburgerstr. 7, 73432 Aalen-Ebnat, Germany

[4]*Howden Axial Fans AB*
SE-351 87, Växjö, Kvarnvägen 18, Sweden

SUMMARY

Aeroacoustic wind tunnels require not only appropriate passive sound attenuation measures but also low noise fans. Due to innovative manufacturing methods large fans may now be equipped with highly skewed rotor blades – a proven method for noise reduction. In this case study we describe the development steps of a complete axial fan stage comprising rotor and guide vanes at model scale level.

The reliable prediction of the acoustic emission of a fan is still computationally extremely expensive. Therefore, to achieve the low noise target a substantial skew of the rotor blades and a combination of the counts of blade and guide vanes for minimizing mode propagation in the duct system are chosen. Naive blade skew can introduce 3D-flow effects with a substantial degradation of efficiency. Therefore, the rotor blade shape and the guide vanes are optimized aerodynamically via an automated CFD-RANS-based optimization scheme.

The model scale fan stage is manufactured and its aerodynamic and acoustic characteristics are measured. A comparison with experimental data from a model scale state-of-the-art benchmark wind tunnel fan with unskewed rotor blades reveals that the new optimized design has a considerably larger range of operation with good efficiency and without stall. The sound power emitted by the optimized fan is substantially lower as from the benchmark over the complete range of possible operation.

INTRODUCTION

An axial fan with guide vanes for wind tunnel application is to be designed for a specified duty characteristic. Primary objective of the design effort is a substantial noise reduction as compared to the baseline design as in Fig. 1 while maintaining its good aerodynamic efficiency. Numerical methods for aerodynamic performance prediction are well established in the turbo machinery community and valuable tools for "numerical" experiments, e.g. the analysis and optimization of an initial design. Reynolds-averaged Navier-Stokes (RANS) codes are regarded as a mature tool, and unsteady methods such as large eddy simulation (LES) and the Lattice-Boltzmann method (LBM) gain ground because of the demand from aero-acousticians engineers. Nevertheless, the reliable prediction of the acoustic emission of a particular fan design is still computationally extremely expensive and for industrial projects not often affordable.

The paper reports a "hybrid" design strategy: Firstly, two design features are incorporated into the new design purely because of acoustic reasoning: (i) a substantial skew of the rotor blades and (ii) a combination of the counts of blade and guide vanes minimizing mode propagation in the duct systems are chosen. Naive blade skew can introduce 3D-flow effects with a substantial degradation of efficiency. Therefore, in a second step the preliminary shape of rotor blades and guide vanes are designed with an enhanced - but still semi-analytical - blade element momentum method (BEMM). In a third step this preliminary blade geometry is optimized with respect to aerodynamic performance via an automated CFD-RANS-based optimization scheme. And finally, in the forth step, the resulting optimized design is manufactured at model scale level and tested experimentally. Especially the effectiveness of the noise reducing features and the optimization is to be confirmed in this last step. This paper concentrates on the automated CFD-RANS-based optimization scheme and on the experimental results. The enhanced blade-element momentum method (BEMM) has been described elsewhere, Carolus and Starzmann [1].

DESIGN METHOD

Design point analysis and resulting decisions

Two non-dimensional design point in terms of the flow coefficient φ and the total-to-total pressure coefficient ψ_{tt}

$$\varphi = Q \Big/ \left(\frac{\pi^2}{4} D^3 n \right), \; \psi_{tt} = \Delta p_{tt} \Big/ \left(\frac{\pi^2}{2} D^2 n^2 \rho \right) \qquad (1, 2)$$

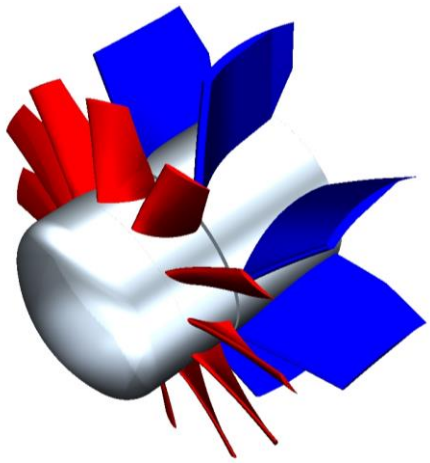

Fig. 1: Baseline fan stage for wind tunnel application

are specified as DP1= (φ = 0.240/ψ_{tt} = 0.274) and DP2 = (φ = 0.294/ψ_{tt} = 0.208). It was decided to mainly focus on DP1 which is the design point with the lower flow coefficient and hence more prone to aerodynamic stall. According to our experience DP2 will be fulfilled automatically, provided that the characteristic curve of the fan does not decay too steeply at higher flow rates. One measure to generate flat characteristic curves is to use a small hub-to-tip ratio ν. Therefore, a value of ν = 0.45 was chosen.

Features for minimum sound emission

An overview of sound sources and features for sound reduction of impellers is e.g. provided in Carolus and Stremel [2], partly based on the early findings by Ffowcs Williams and Hall [3], Wright and Simmons [4] and Tylor and Sofrin [5]. The reduction of *some* sources require design features which are difficult to be realized; e.g. a very small blade tip gap (Zhu, [6]), and a very thin blade trailing edge. Other sources are associated with the interaction of secondary flows and flow separations with the blade. The reduction of these sound sources goes hand in hand with the aim of minimizing flow losses. Hence, these sound sources will be addressed automatically via the subsequent aerodynamic optimization.

One of the remaining sound sources is the interaction of the incoming turbulence with the blade leading edge. This sound mechanism is particularly effective when the impeller faces a highly turbulent inflow. A measure to reduce this sound mechanism is skewing the blade leading edges. The term "skew" refers to a blade which has - in terms of aircraft wing design - sweep and dihedral. A wing is said to have sweep when tilted in, and dihedral, when tilted perpendicular to the flow direction. For an unskewed blade, it is generally assumed that the sound power P_{ac} rises with the fifth power of the incoming relative velocity w. A simple model for estimating the sound reduction due to a skewed leading edge assumes that only the velocity component normal to the blade leading edge w_n is acoustically relevant. This velocity component decreases with increasing skew angle λ:

$$P_{ac} \sim w_n^5 = \left(w \cdot \cos\lambda\right)^5 \Rightarrow P_{ac} \sim \left(\cos\lambda\right)^5 \tag{3}$$

Given these assumptions, the difference in sound power level emitted from a skewed and an unskewed impeller becomes

$$\Delta L_W = 50 \cdot \log_{10}\left(\cos\lambda\right). \tag{4}$$

A similar analysis holds true for the trailing edge noise. A constant blade skew angle of 45°, for instance, would lead to a theoretical sound reduction of approx. 7 dB. However, constant skew angles are rarely realized because such blades require more space in axial direction and have unfavorable locations of the center of gravity. The skew angles selected for this project are chosen to vary along the blade span and change from negative skew (i.e. in the direction of w) near the hub to positive skew (i.e. against the direction of w) near the tip. Altogether, the theoretical sound reduction of this skew strategy is almost equivalent to the 45° example.

Besides the reduction of sound sources, the suppression of sound propagation represents another effective measure to reduce the sound power perceived in the far field. According to a model by Tylor and Sofrin [5], the propagation of acoustic modes, related to tones at blade passing frequency, into the attached ducts is affected by the number and combination of rotor and guide vanes. For the condition of the envisaged full scale fan with 8 m rotor diameter operating with approximately 300 rpm, Tylor and Sofrin's model suggest eleven rotor blades and seven stator vanes. This combination has the potential to convert relevant modes from propagating into evanescent and hence to reduce some tonal components of the sound emitted. It is important to note, however, that the success of this feature may not be confirmed in model scale tests, since it is a function of acoustic parameters like wave length and Mach number, which differ substantially at model scale level.

Preliminary design based on an enhanced blade element momentum method [BEMM]

The blade element momentum method (BEMM) employed is encoded in our in-house code dAX (in its current version 10.15), see also [1]. BEMM is a quasi 2D design method for turbo machinery. It treats the blade as a stack of isolated airfoil sections and assumes two-dimensional flow around those sections. The flow around the 2D sections is obtained by the integrated open source software XFOIL. Some 3D effects are taken into account via ensuring radial equilibrium of the fluid elements at the rotor outlet and by compensating the lift reduction due to blade skew. Important user inputs are the design point, the hub-to-tip ratio, the number of blades, and the spanwise load distribution.

dAX also allows the design of guide vanes. The guide vane inlet angles are equivalent to the predicted flow angles downstream of the impeller to minimize shock losses. At the outlet, the flow angle is supposed to be 90° (i.e. parallel to the axis of rotation). Since the flow does not entirely follow the guide vanes ("slip"), empirical corrections are applied to compute the required blade angle which is always larger than 90°.

Final design based on CFD-optimization

Due to simplifying assumptions (e.g. 2D flow around a blade segment) and potentially non-optimal user input (e.g. the load distribution), the fan designed with dAX is only regarded as a starting point for the CFD-based aerodynamic optimization. In general, "optimization" means more than just "improvement". It is a mathematical method to make systems (here fans) as good as possible and proves that no better solutions exist for a given parameterization of the fan geometry.

The free optimization parameters for the fan are

- impeller blade stagger angle[1]
- impeller blade chord length[1,2]
- impeller blade camber[1,2]
- guide vane inlet angle[1]
- guide vane outlet angle
- guide vane bending radius

The optimization algorithm selected for this project was the Simplex method by Nelder and Mead [7]. All optimization methods require a target function (*TF*) to be maximized or minimized. In the present case, the target is to maximize the total-to-total efficiency η_{tt} of the fan taking into account a penalty term for the violation of the design point. While exceeding the targeted pressure coefficient $\psi_{tt,target}$ is acceptable (the penalty term equals zero in that case), the penalty term rises if the actual pressure coefficient $\psi_{tt,actual}$ falls below the target:

$$TF = \eta_{tt} - \max\left\{\psi_{tt,target} - \psi_{tt,actual}, 0\right\} \tag{5}$$

η_{tt} and $\psi_{tt,actual}$ are determined by CFD-simulations.

The software used for the CFD simulations was OpenFOAM (version 3.0.1) and the computational grids were generated with the software cfMesh 1.2. A stationary flow field was assumed meaning that the Reynolds-averaged Navier-Stokes (RANS) equations had to be solved. The turbulence model used was *k*-ω SST (shear stress transport). The impeller and the guide vanes were simulated separately. Each grid consisted of approximately one million nodes with local refinements near the blade and in the boundary layers. The impeller was simulated first yielding the shaft power, the

[1] defined at three equidistant locations between hub and tip, polynomial interpolation in between

[2] of 4-digit NACA sections

pressure rise and the downstream velocity profile. Afterwards, the guide vanes were simulated yielding the pressure recovery from the swirl and eventually the overall pressure rise of the fan. As usual in RANS simulations, only one blade or vane (not the full rotor or stator) was simulated assuming periodicity at the sides of the flow channel. The other boundary conditions were

- no slip at the walls (hub, shroud, impeller blade, guide vane)
- rotational speed of the impeller hub and impeller blade
- ambient pressure at the outlet
- velocity profile at the inlet
  - impeller inlet: block profile of the axial velocity
  - guide vane inlet: circumferentially averaged outflow profile of the impeller

Initially, the impeller and the guide vanes were optimized simultaneously. After some hundred of CFD-simulations, the optimization process was terminated, the design of the impeller was frozen and only the guide vanes were further optimized.

TEST RIGS

At the University of Siegen the standard diameter of model scale axial fan rotors is 300 mm. For the model scale measurements two different test rigs were employed. Fig. 2 shows schematically the chamber test rig for aerodynamic performance testing according to the German standard DIN 24163 [8]. The total-to-static pressure rise equals the pressure differential of the ambient atmosphere to the chamber pressure Δp_{ch}. The volume flow rate is determined from Δp_{nozzle} at the calibrated flow rate metering nozzle. An external electric motor with its integrated torque shaft is used as the fan drive. Prior to all fan measurements the frictional torque due to all bearings between torque shaft and fan rotor is determined with the fan rotor being removed.

The total-to-total pressure rise Δp_{tt} is defined as

$$\Delta p_{tt} = p_{t2} - p_{t1} = \left(p_2 + \frac{\rho}{2} c_2^2 \right) - \left(p_1 + \frac{\rho}{2} c_1^2 \right) \tag{6}$$

where the indices 1 and 2 denote locations upstream and downstream of the fan, respectively. p_t is the total pressure, p is the static pressure and c is the velocity. In the chamber test rig used here p_{t1} is the static pressure in the settling chamber and is measured directly. p_{t2} needs the determination of the outlet velocity c_2. As common practice, c_2 is obtained as the volumetric average

$$c_2 = \frac{Q}{A}, \tag{7}$$

where A is the annular through flow area downstream of the guide vanes. The corresponding total-to-total efficiency is

$$\eta_{tt} = \frac{Q \cdot \Delta p_{tt}}{P_{shaft}} \tag{8}$$

with P_{shaft} being the shaft power driving the impeller.
Acoustic measurements are conducted on a duct test rig for fans according to ISO 5136 [9], Fig. 3. The impeller takes the air from a large plenum, designed as a semi-anechoic chamber (i.e. absorbing walls and reflecting ground) and exhausts into a duct with an anechoic termination. The downstream sound power level L_{w4} in the exhausting duct (duct sound power level) is

$$L_{W4}(f) = L_{p4}(f) + 10\log_{10} \frac{A_K}{A_0} \tag{9}$$

with the reference area A_0 = 1 m^2. The sound pressure levels L_p are determined with reference to the standard reference pressure $p_0 = 2 \cdot 10^{-5}$ Pa.

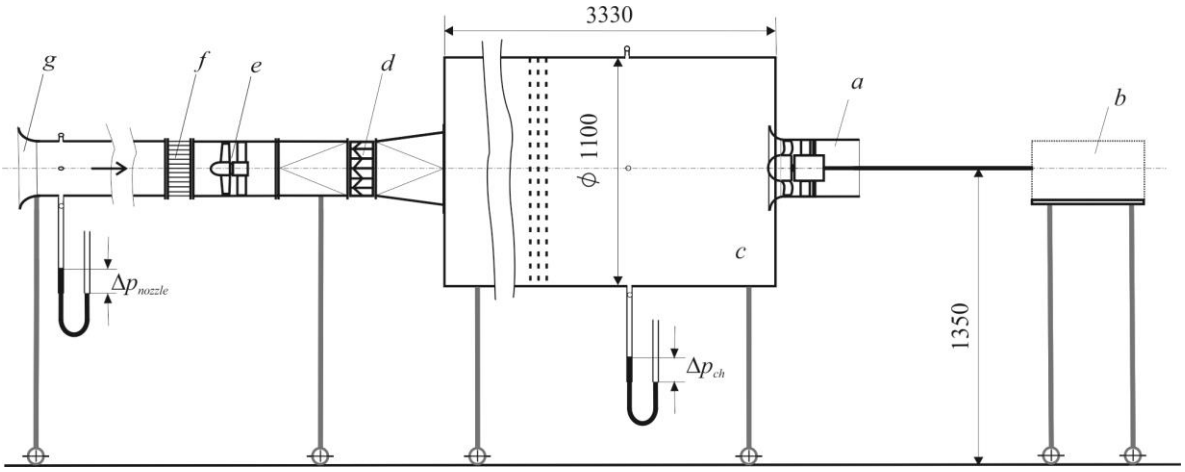

Fig. 2: Aerodynamic and aeroacoustic chamber test rigs at the University Siegen (schematically); (a) fan assembly; (b) electric motor with integrated torque meter, (c) settling chamber with internal screens, (d) adjustable throttle, (e) auxiliary fan, (f) flow straightener, (g) volume flow rate metering nozzle

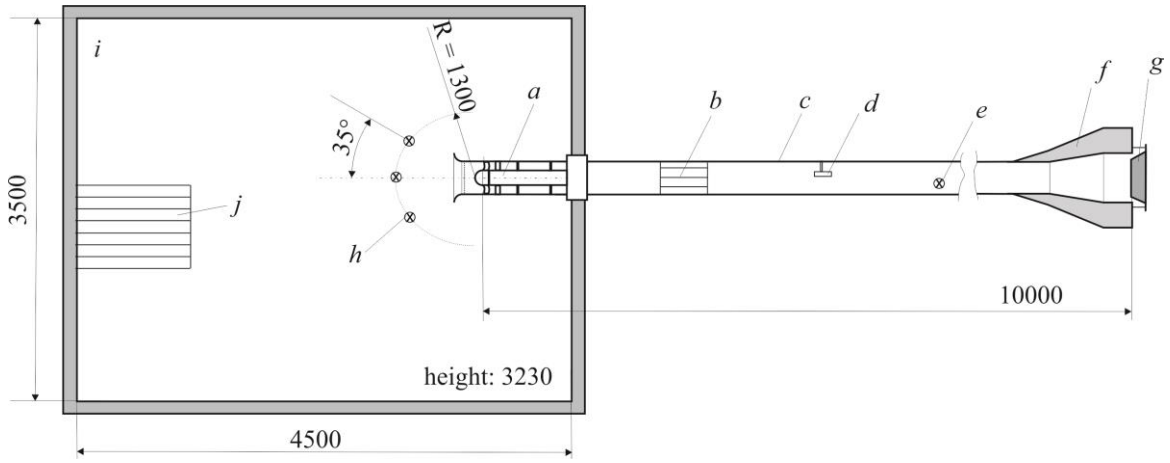

Fig. 3: Duct test rig at the University Siegen with semi-anechoic chamber (top view, schematically); (a) fan assembly, (b) star flow straightener, (c) duct, (d) induct microphone, (e) hot film mass flow meter, (f) anechoic termination, (g) adjustable throttle, (h) free field microphones, (i) semi-anechoic chamber, (j) air inlet grid in reflecting ground

L_{p4} is measured in the duct by a single microphone mounted four meter downstream of the impeller with a slit tube and a nose cone to cancel out pseudo sound and avoid duct mode effects. A_K is the cross-sectional area of the duct.

The upstream inlet side sound pressure level L_{p5} is measured in the free field of the semi-anechoic chamber. In a pre-study 16 microphones were placed on a parallelepiped enclosing the bellmouth fan inlet nozzle and the reflecting ground according to ISO 13347-3 [10]. This costly method eventually was replaced by a set of three microphones, placed on a hemispherical arc around the inlet in a distance of r = 1.3 m from the fan's spinner and 1350 mm above ground. The measurement surface area was taken as $A_M = 2\pi r^2$ and the sound power obtained by

$$L_{W5}(f) = 10\log_{10}\left(\frac{1}{3}\sum_{i=1}^{3} 10^{0{,}1 \cdot L_{p5,i}(f)}\right) + 10\log_{10}\frac{A_M}{A_0}, \qquad (10)$$

again with the reference area $A_0 = 1\ \mathrm{m}^2$. The volume flow rate is controlled by an adjustable throttle downstream of the termination and is determined by a calibrated hot film probe in the duct. No auxiliary fan is incorporated in order to avoid any acoustic contamination. All overall sound levels are the sum of narrow band levels from approx. 100 to 10 kHz, with 100 Hz corresponding to the low-frequency bound of the anechoic chamber.

The *specific* overall sound power level is defined as

$$L_{W,spec} = L_W - 10\log_{10}\left(\frac{Q\ [\mathrm{m}^3/\mathrm{s}]}{1\ \mathrm{m}^3/\mathrm{s}}\right) - 20\log_{10}\left(\frac{\Delta p_{tt}\ [\mathrm{Pa}]}{1\ \mathrm{Pa}}\right)\ \mathrm{dB}. \qquad (11)$$

RESULTS

Remark: Reynolds number correction

It was decided to perform the simulations and hence the complete optimization at model scale, i.e. $D = 0.3$ m and $n = 2900$ to 3000 rpm. As a consequence, the simulation results are compatible to the experimental model scale tests planned but not to the full scale version of the fan, wherefore the performance will most probably be underestimated. However, Ackeret's Reynolds number correction (Muhlemann [11]) is employed for predicting the aerodynamic performance of the full-scale fan:

$$\eta_{tt,B} = \eta_{tt,A} + \left(1 - \eta_{tt,A}\right) \cdot V \cdot \left(1 - \left(\frac{\mathrm{Re}_A}{\mathrm{Re}_B}\right)^{\alpha}\right) \qquad (12)$$

The factor V represents the portion of the losses that is dependent on the Reynolds number Re. The exponent α determines the sensitivity with which the efficiency varies with Reynolds number.

Design

Fig. 4 depicts a 3D view of the optimized fan stage. The left picture shows the final fan assembly comprising impeller and guide vanes. The right picture compares the final optimal impeller to the initial impeller designed with the BEMM. It can be seen that optimization modified the blade in detail but not overall.

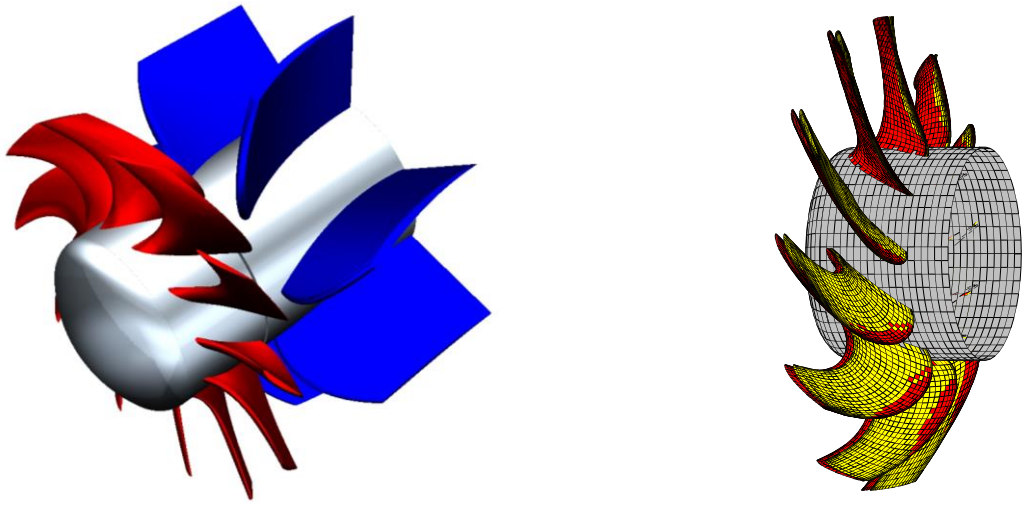

Fig. 4: 3D views of the optimized fan stage. The yellow surface in the right picture represents the initial design based on the blade element momentum method, the red the optimized

Fig. 5 shows the CFD-predicted characteristic curves. The figure also contains the anticipated performance data of the full scale version (D = 8 m, n = 313 rpm), based on the scaling law, eq. (12). Not knowing the exact values of V and α, an efficiency band corresponding to V varying between 50 and 70 % and α between 0.2 and 0.5 is plotted. Fig. 5 also depicts the targeted design points DP1 and DP2. The optimized fan meets both with a safety margin.

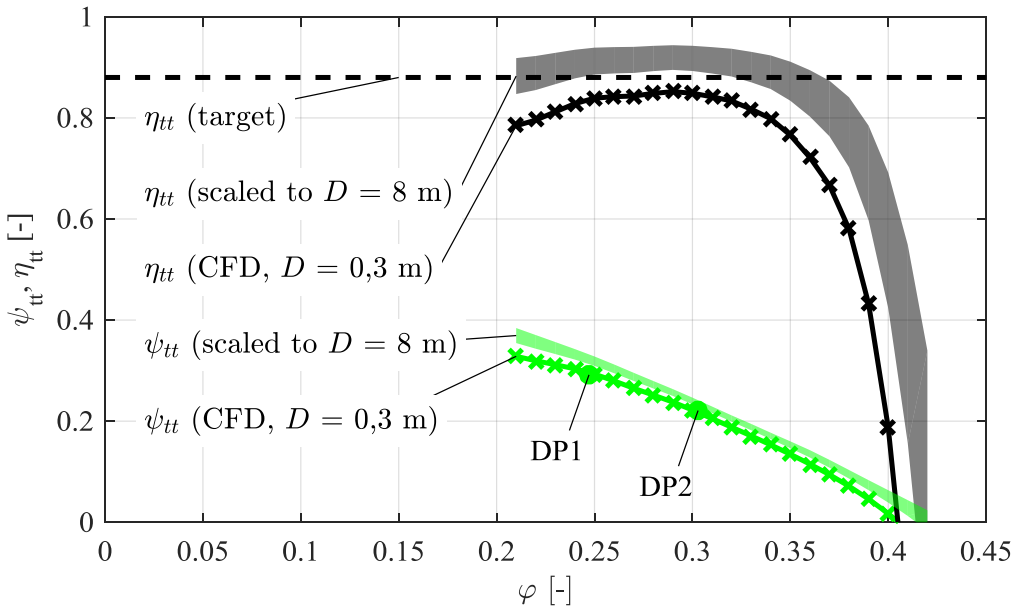

Fig. 5: Predicted aerodynamic performance curves of the optimized fan (model scale and full scale Reynolds number corrected)

Experimental results: Aerodynamic and acoustic characteristics

A comparison of measured performance of both fan stages is presented in Figs. 6 and 7. The measured aerodynamic characteristics are non-dimensionalized utilizing the definitions in eqs. (1), (2) and (8), the overall sound power levels are specific according to eq. (12).

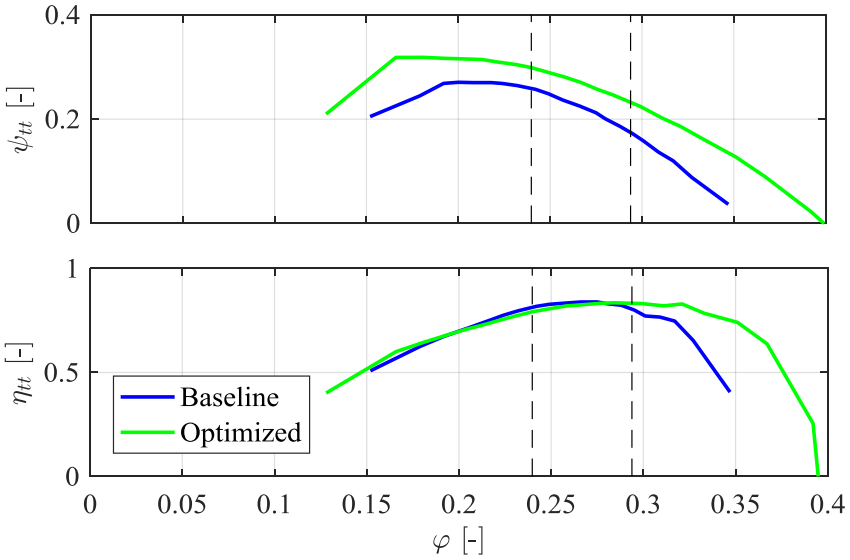

Fig. 6: Non-dimensional total-to-total aerodynamic characteristics from model-scale tests, tip gap: 0.15% of rotor diameter D

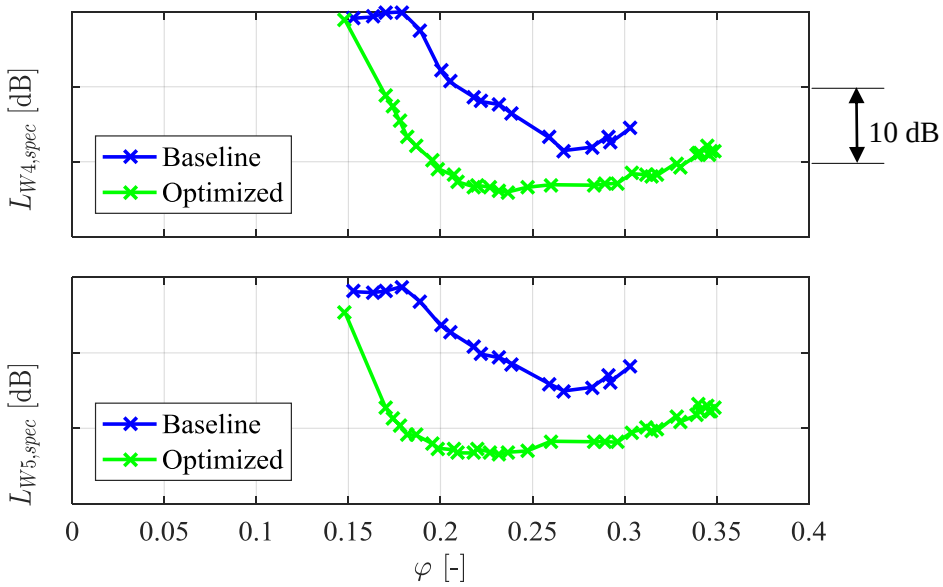

Fig. 7: Specific overall sound power characteristics from model-scale tests;
upper: in pressure side of the duct, lower: at the free suction side; tip gap: 0.45 mm or 0.15% of rotor diameter D

As compared to the baseline the optimized fan has a larger total-to-total pressure rise in the complete range of operation. At the same time, the stall point is moved to a smaller volume flow rate, with the effect of a wider range of stall-free operation. This particular effect of blade skew has been observed by many authors, e.g. already in 1999 by Beiler and Carolus [12]. Within measurement accuracy the total-to total peak efficiency of both fan stages is identical, i.e. optimization was successful in compensating for the set blade skew.

Fig. 7 presents the specific pressure side duct sound power level $L_{W4,spec}$ and the suction side free field level $L_{W5,spec}$. The sound emitted by the new fan is remarkably lower for all operating points. Moreover, the optimized fan offers a much larger range of low-noise operating points

Experimental results: Acoustic spectra

Fig. 8 presents a comparison of narrow band sound pressure spectra of both fans at three different operating points (φ =0.18, 0.24 and 0.29). The latter two correspond to the two initial design points DP1 and DP2. It is important to note that the spectra stem from the average of all three free field suction side microphone sound *pressure* signals without any normalization in the sense of a specific value. Moreover, they are obtained at a rotor speed n = 2900 rpm for both fans.

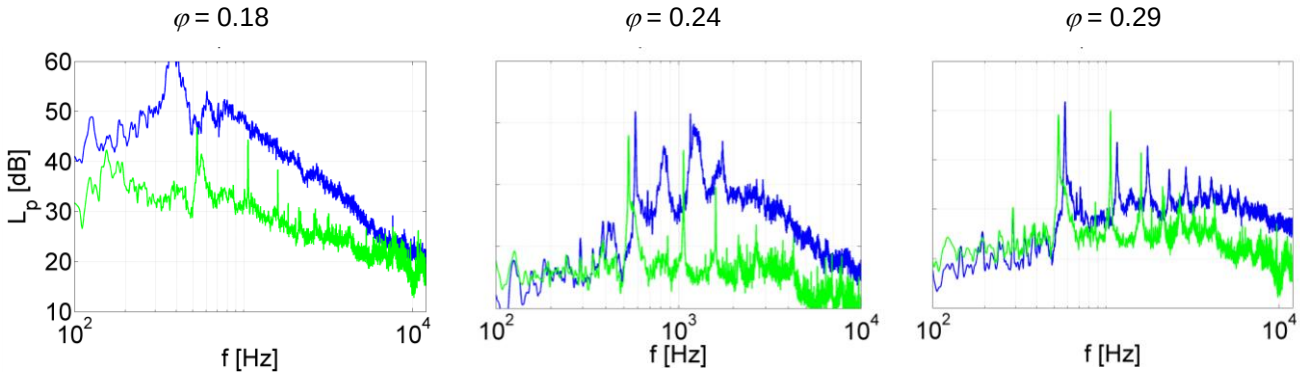

Fig. 8: Comparison of suction side sound pressure (not power!)
spectra of baseline (blue) and optimized (green) fan, operated at three different working points

Again, the differences between the two fans are remarkable: At the high flow rate regime ($\varphi = 0.29$) the optimized fan is superior in the higher frequency range. In contrast, at a low flow rate ($\varphi = 0.18$) the baseline fan emits substantially more low frequency sound as the optimized. Although clearly not stalled the baseline fan obviously suffers from local flow separation in a substantial portion of its performance characteristic.

Experimental results: On the origin of BPF-related tones

If not buried in high levels of broad band sound as in the low flow range regimen, the BPF-related peaks in the spectra are clearly visible. The baseline fan rotor has 12, the optimized 11 blades. Hence, the blade passing frequency for the baseline fan is *BPF* = 12*2900/60 Hz = 580 Hz, for the optimized *BPF* = 11*2900/60 Hz = 531 Hz.

There are two main mechanisms that are responsible for the generation of BPF-related tones: (i) rotor-stator-interaction, (ii) spatially non-uniform inflow ingested by the fan. To a certain degree, rotor-stator-interaction can be controlled by geometrical details of the blade and guide vanes (e.g. blade skew) and by the geometric distance between rotor and stator. As pointed out earlier, the propagation of acoustic modes related to rotor-stator-interaction can be affected by an appropriate match of the number of rotor blades and guide vanes. The second mechanism is not very well-known: Sturm [13] and Sturm and Carolus [14, 15] detected that practically in any large plenum, from which a fan is taking air from, a slow but large-scale room airflow is induced, Fig. 9. This distorted inflow is ingested by the fan and interacts with the rotating blades, causing fluctuating blade forces and eventually tonal sound. This was found to be true even if the size of the plenum equals or exceeds the standards for test rigs. One way to eliminate the encounter of large scale inflow distortions with the fan is an upstream flow conditioner, in essence a turbulence control device, flange mounted to the bell mouth nozzle.

To discriminate between rotor-stator-interaction and spatially non-uniform inflow caused by the plenum of the test rig we repeat the acoustic measurements with a hemispherical flow conditioner (HFC) mounted upstream of the fan, Fig. 10. The HFC is made of a 30 mm thick layer of a flexible honeycomb structure and a wire mesh [14]. Experiments proved that its pressure loss, acoustic damping and self noise are negligible.

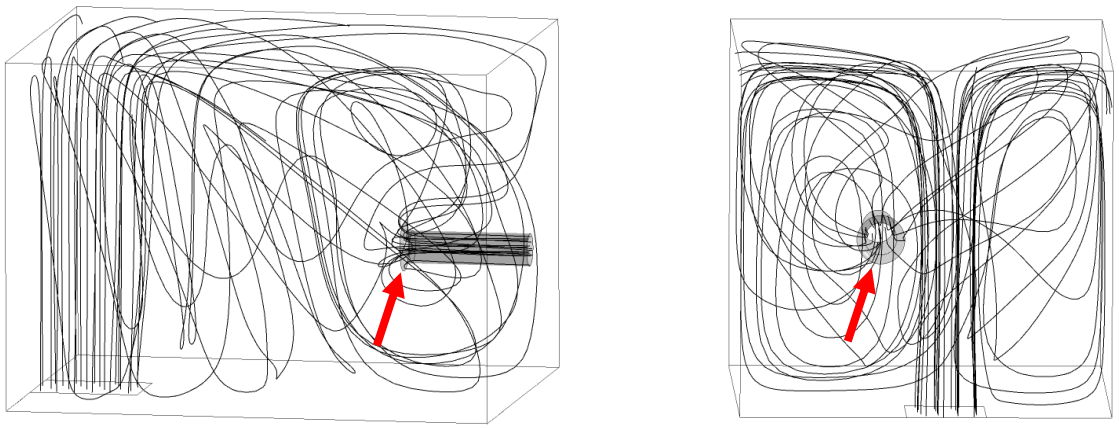

Fig. 9: Flow conditions inside the anechoic chamber at the University of Siegen: streamlines starting from the flow inlet from two different points of view; RANS simulation, from Sturm and Carolus [14]; the red arrows indicate the bellmouth inlet nozzle

Fig. 11 shows a detail of the spectrum comprising the BPF-related tones including some higher harmonics. It becomes evident that a substantial portion of the tones is indeed attributed to the inhomogeneous inflow generated in the inlet plenum. With the distortions eliminated by the HFC the BPF-related amplitudes of both fans are similar, with the exception at 3x BPF, where the

amplitude is lower for the optimized fan. As pointed out earlier, the chosen combination of blade/vane numbers for minimizing acoustic mode propagation can not be validated in model scale tests.

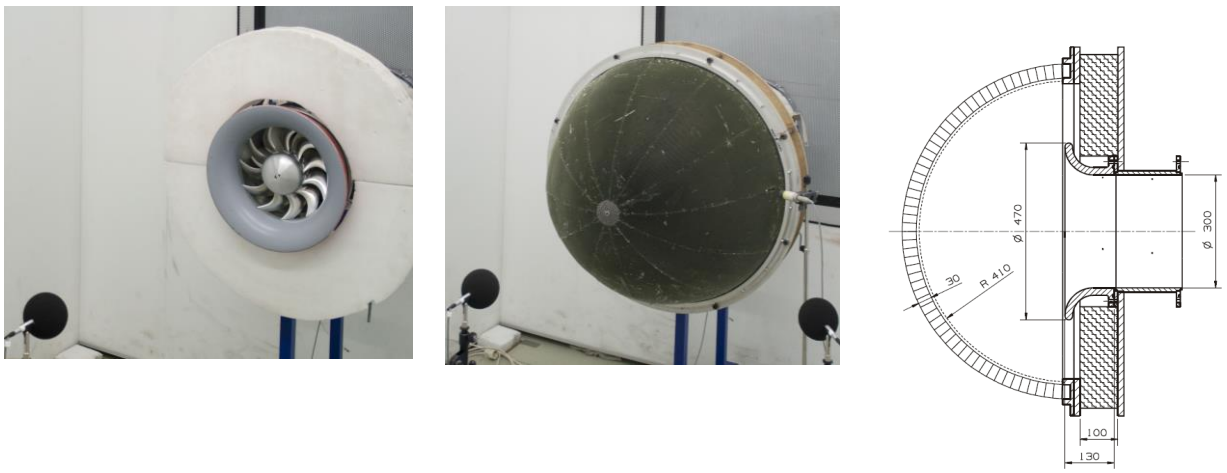

Fig. 10: Left: Free inflow, middle and right: Hemispherical flow conditioner (HFC) upstream of the fan rotor

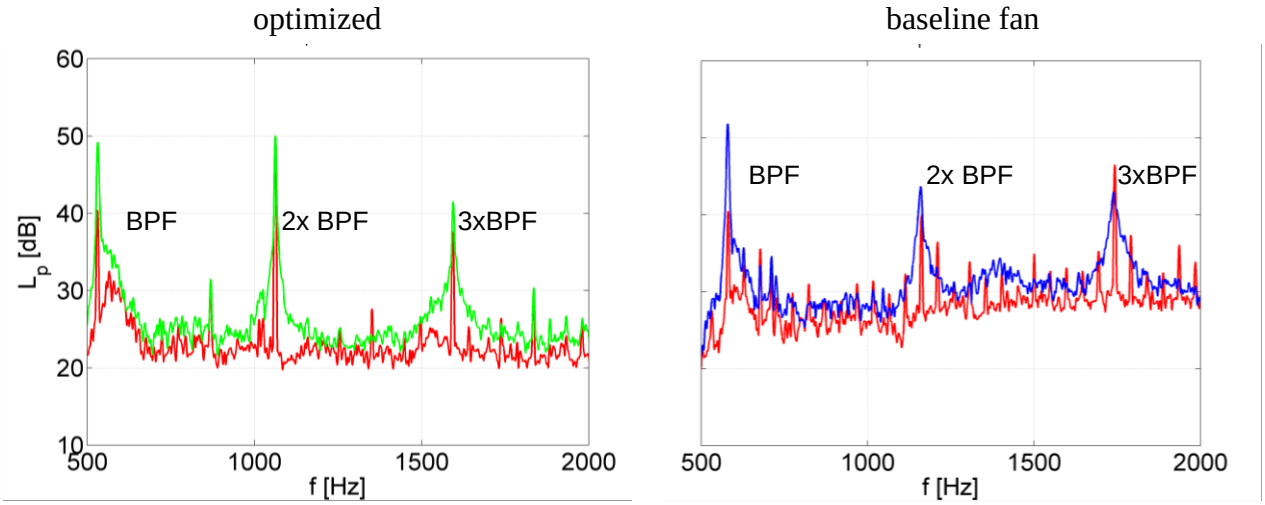

Fig. 11: Detail of the suction side sound pressure spectra from the optimized (green) and baseline fan (blue) without hemispherical flow conditioner (HFC) and with HFC (red); $\varphi = 0.29$, $n = 2900$ rpm

SUMMARY AND OUTLOOK

For a set of given specifications a new wind tunnel fan comprising rotor and stator with guide vanes was designed and optimized. Key features for noise reduction are a substantial skew of the rotor blades and a careful selection of the number of rotor and stator blades. Great effort has been made in a subsequent simulation-based optimization to maximize efficiency and further weaken potential aerodynamic noise mechanisms.

Model scale tests showed that, when compared to the baseline, the optimized fan has a larger total-to-total pressure rise in the complete range of operation. At the same time, the stall point is moved to a smaller volume flow rate, with the effect of a wider range of stall-free operation. Within measurement accuracy the total-to total peak efficiency of both fan stages is identical, i.e. optimization was successful in compensating for the set blade skew. The sound emitted by the optimized fan is remarkably lower for all operating points. Moreover, the optimized fan offers a much larger range of low-noise operating points. A substantial portion of the blade passing

frequency-related tones is attributed to the inhomogeneous inflow generated in the inlet plenum. With the distortions being eliminated with the aid of a flow control device mounted upstream of the fan the BPF-related amplitudes of both fans are similar, with the exception at 3x BPF, where the amplitude is lower for the optimized fan.

The next step in validating these results would be manufacture and testing medium and full scale versions of the fans. It will allow answering the important question, how the performance from the comparably small model translates into full scale. Aerodynamic scaling laws are found to be reliable for many years, whereas acoustic scaling of fan noise is probably more difficult.

ACKNOWLEGEMENT

The authors want to thank Dipl.-Ing. B. Homrighausen. Without his countless hours of 3D CAD design work, supervising the manufacture of the model scale fans and measuring the fan performance the project would not have been possible.

REFERENCES

[1] Carolus, T., Starzmann, R., **2011**, "An Aerodynamic Design Methodology for Low Pressure Axial Fans with integrated Airfoil Polar Prediction", *Proc. ASME TurboExpo 2011,* Vancouver, Canada

[2] Carolus, T., Stremel, M., **2000**, Sichelschaufeln bei Axialventilatoren. HLH Bd. 51, August, pp. 33 - 39

[3] Ffowcs Williams, J.E., Hall, L.H., **1979**, "Aerodynamic sound generation by turbulent flow in the vicinity of a scattering half plane". J. Fluid Mech., vol. 40, part4, p. 657-670

[4] Wright, T., Simmons, W.E., **1990**, "Blade sweep for low-speed axial fans". ASME J. of Turbomachinery, vol. 112, pp. 151-158

[5] Tylor, J. M., Sofrin, T. G., **1962**, "Axial flow compressor noise studies", *Trans. Soc. Automotive Eng.*, 70, pp. 309-332

[6] Zhu, T.: On the Flow Induced Tip Clearance Noise in Axial Fans, 2016, Dr.-Ing. Diss. Univ. Siegen, Shaker Verlag **2016**, ISBN 978-3-8440-4802-5

[7] Nelder, J. A., Mead, R., **1965**, "A Simplex Method for Function Minimization", *Computer Journal*, 7, pp. 308-313

[8] DIN 24163-2: Ventilatoren, Teil 2: Leistungsmessung - Normprüfstände (Fans, Part 2: Performance Tests - Standardized Test Rigs), **1985**

[9] ISO 5136: Acoustics - Determination of Sound Power Radiated into a Duct by Fans and Other Air-Moving Devices - In-duct Method, **2003**

[10] ISO 13347-3: Industrial fans - Determination of Fan Sound Power Levels Under Standardized Laboratory Conditions, Part 3: Enveloping Surface Methods, **2004**

[11] Muhlemann, E., **1948**, "Zur Aufwertung des Wirkungsgrads von Überdruckwasserturbinen", Bauzeitung, 66, pp. 331-333

[12] Beiler, M., Carolus, T., **1999**, "Computation and Measurement of the Flow in Axial Flow Fans with Skewed Blades". ASME J. of Turbomachinery, Jan. 1999, Vol. 121

[13] Sturm, M., **2016**, "Tonal Noise of Axial Fans Induced by Large-Scale Inflow Distortions", Shaker Verlag Aachen, also PH.D. thesis at the University of Siegen 2015

[14] Sturm, M., Carolus, T. , **2012**, "Tonal Fan Noise of an Isolated Axial Fan Rotor due to Inhomogeneous Coherent Structures at the Intake". Noise Control Engr. J. 60 (6), November-December, pp. 699-706

[15] Sturm, M., Carolus, T., **2013**, "Impact of the Large-Scale Environment on the Tonal Noise of Axial Fans". Proc. IMechE Part A, J. Power and Energy 227(6) 703-710